Natural Resources Research, Vol. 31, No. 3, June 2022 (© 2022)
https://doi.org/10.1007/s11053-022-10051-w

Original Paper

A Novel Approach to Uncertainty Quantification in Groundwater Table Modeling by Automated Predictive Deep Learning

Abbas Abbaszadeh Shahri,[1,2,4] Chunling Shan,[1,3] and Stefan Larsson[3]

Received 20 September 2021; accepted 10 March 2022
Published online: 12 April 2022

Uncertainty quantification (*UQ*) is an important benchmark to assess the performance of artificial intelligence (*AI*) and particularly deep learning ensembled-based models. However, the ability for *UQ* using current *AI*-based methods is not only limited in terms of computational resources but it also requires changes to topology and optimization processes, as well as multiple performances to monitor model instabilities. From both geo-engineering and societal perspectives, a predictive groundwater table (*GWT*) model presents an important challenge, where a lack of *UQ* limits the validity of findings and may undermine science-based decisions. To overcome and address these limitations, a novel ensemble, an automated random deactivating connective weights approach (*ARDCW*), is presented and applied to retrieved geographical locations of *GWT* data from a geo-engineering project in Stockholm, Sweden. In this approach, the *UQ* was achieved via a combination of several derived ensembles from a fixed optimum topology subjected to randomly switched off weights, which allow predictability with one forward pass. The process was developed and programmed to provide trackable performance in a specific task and access to a wide variety of different internal characteristics and libraries. A comparison of performance with Monte Carlo dropout and quantile regression using computer vision and control task metrics showed significant progress in the *ARDCW*. This approach does not require changes in the optimization process and can be applied to already trained topologies in a way that outperforms other models.

KEY WORDS: Uncertainty quantification, Automated modeling, *ARDCW*, Groundwater, Sweden.

INTRODUCTION

Groundwater is one of a nation's important natural resources but its incorporation with level in terms of groundwater table (*GWT*) dedicates a nonlinear time-dependent concern in many geo-engineering projects (Hu & Jiao, 2010; Parry et al., 2014; Tang et al., 2017; Salvo et al., 2020). Modeling of *GWT* is applied to conceptualize and integrate knowledge on the natural and engineering disciplines to address a range of issues in different spatial and temporal scales (Mohammadi, 2009; Yeh et al., 2015; Bizhanimanzar et al., 2019). However, due to several embedded nonlinear complexities in the system, modeling of *GWT* is an inherently difficult task. Moreover, the sources of uncertainties related to model parameters, underlying conceptual assumptions, structure of model, geological condi-

[1] Division of Rock Engineering, Tyréns AB, Stockholm, Sweden.
[2] Johan Lundberg AB, Uppsala, Sweden.
[3] Division of Soil and Rock Mechanics, KTH Royal Institute of Technology, Stockholm, Sweden.
[4] To whom correspondence should be addressed; e-mail: abbas@johanlundberg.se

1520-7439/22/0600-1351/0 © 2022 The Author(s)

tions, observed spatial data (i.e., lack of data on natural variability), and steady-state *GWT* should be considered (Beven & Binley, 1992; Stedinger et al., 2008; Yeh et al., 2015; Hauser et al., 2017). As a result, computer code models have primarily been developed over simplified assumptions using long-term time series through different approaches, such as statistical techniques, approximation methods and numerical analyses (Rushton, 2003; Yan et al., 2018). Therefore, evaluating the robustness and accuracy performance of a predictive *GWT* model using uncertainty quantification (*UQ*) analysis is often required. Nowadays, alternative modern computational artificial intelligent techniques (*AIT*) lead to systematic *UQ* analysis that can be applied effectively to generate a *GWT* model (Guillaume et al., 2016; Sahoo & Russo, 2017; Chen et al., 2020; Wunsch et al., 2020; Yin et al., 2021).

Uncertainty can simply be described as knowledge situations involving imperfect or unknown information (Gärdenfors & Sahlin, 1982). To quantify uncertainty, three sources including physical variability of equipment, data, and model error should be considered (Barford, 1985; Kennedy & O'Hagan, 2001). In the modeling process, methods *UQ* are described in the context of different factors, such as input variabilities, assumptions and approximations, measurement errors, and sparse and imprecise data (Yan et al., 2015). In the literature, statistical techniques, sensitivity analyses, Taylor series approximation, Monte Carlo simulation, numerical estimation, and probability distributions are the most commonly used methods for *UQ* (e.g., Cox & Baybutt, 1981; Glimm & Sharp, 1999; Bárdossy & Fodor, 2001; Uusitalo et al., 2015; Elam & Rearden, 2017; Asheghi et al., 2020). However, when using these techniques for value-based judgements, all sources of uncertainty may not be quantifiable (Morgan & Henrion, 1990). The taxonomy of different methods applied to *UQ* are given in Figure 1.

In statistical techniques, *UQ* is based usually on the estimated variance and determined confidence limits by assuming normally distributed error (e.g., Eisenhart et al., 1983; Cacuci & Ionescu-Bujor, 2004; Jiang et al., 2018; Zhang et al., 2020). Because quantification is most often based on statistical indices (e.g., mean, median, population quantiles) due to limited sample size, estimations must be provided with the associated confidence intervals (Geffray et al., 2019). Therefore, due to underlying foundations, such as measurement errors, material properties, unknown design demand models, and stochastic environments, the applicability of statistical techniques is limited (Taper & Ponciano, 2016). The Taylor series approximation can be used to determine theoretical error bounds but is very complex to derive and it tends to increase quickly the risk of error (Barrio et al., 2011). Monte Carlo is applied mainly to explain the probability density function but it is a complex process and requires several simulations and computational resources when the dataset is large. Therefore, it only provides statistical estimates of results, not exact figures (Atanassov & Dimov, 2008). Results of numerical methods of *UQ*, which are simulated by computer codes, inherently involve error or uncertainty. Such drawbacks can be addressed in part by defining the error magnitude or bound the error in a given simulation (Freitas, 2002). By using probability distributions, accurate information on the uncertainty can be achieved, but infinite extension along either side of the most probable region creates a sophisticated situation that is difficult to interpret (Kabir et al., 2018). Moreover, quantitative measures may bias the description of uncertainty towards the more computational components of the assessment (Bárdossy & Fodor, 2001). Therefore, the concepts and methods used for *UQ* make it difficult to communicate the results effectively. This implies that the analysis for *UQ* through ensemble methods is one of the main benchmarks to assess the performance of complex systems (Vrugt & Robinson, 2007; Zhang et al., 2021), especially in geo-engineering and *GWT* predictive modeling, which often suffer from inadequate experimental or data (e.g., Whitman, 2000; Wu & Zeng, 2013; Sepulveda & Doherty, 2015; Huber, 2016; Li et al., 2018; Chahbaz et al., 2019). Furthermore, computing the contribution of each error component on total uncertainty is difficult and it leads to extreme weighting schemes with applicability that is often questionable. Therefore, no unified applicable methodology exists for combining uncertainties. Because these methods typically yield an estimate of the total variance of measurement values, reliance on statistical variance can produce misleading results that are not readily applicable (e.g., Goodman, 1960; Yager, 1996; Borgonovo, 2006; Farrance & Frenkel, 2012).

Due to the revolution of different types of *AITs* in recent years, and deep neural networks (*DNNs*) in particular, these mechanisms have shown impressive state-of-the-art performance on a wide

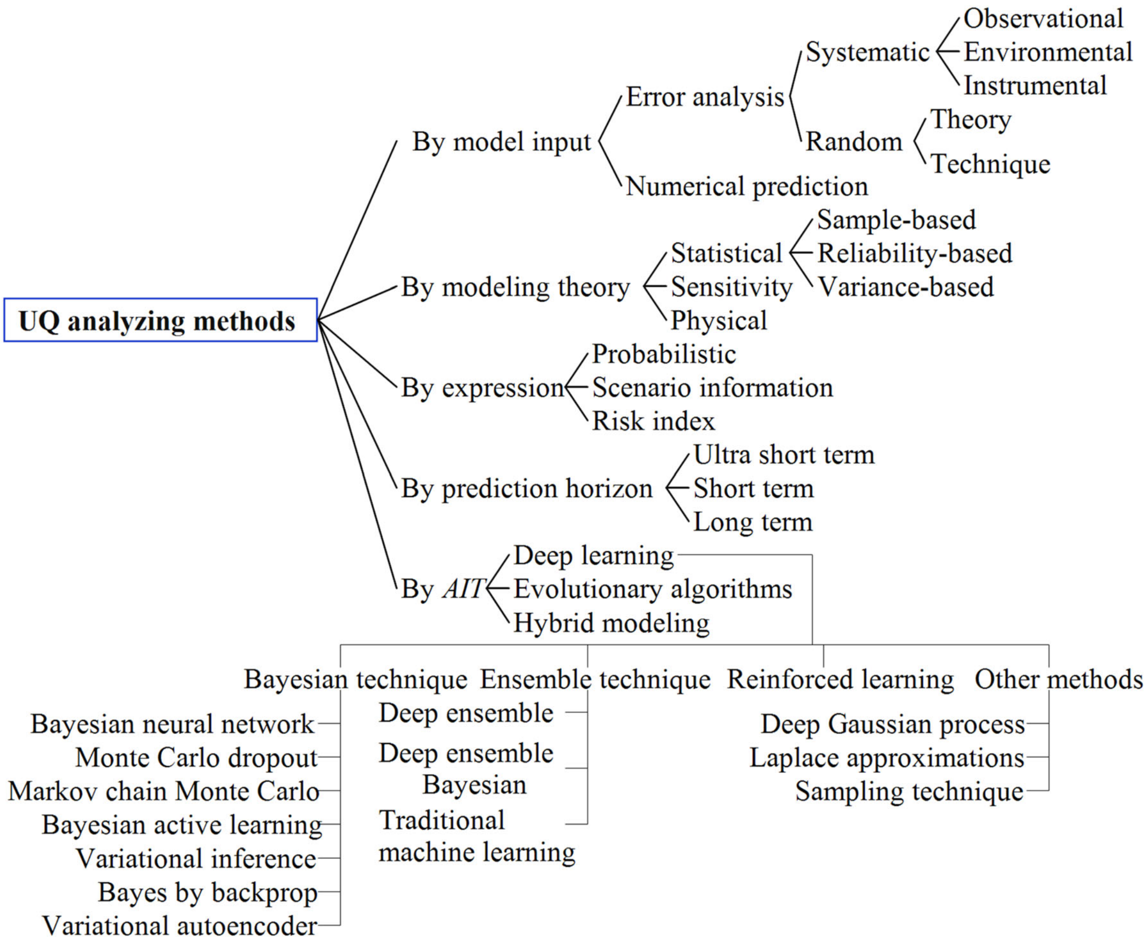

Figure 1. Taxonomy of *UQ* methods.

variety of engineering tasks dealing with challenging scientific data analysis and *UQ* problems (e.g., Vrugt & Robinson, 2007; Chahbaz et al., 2019; Abbaszadeh et al., 2020; Hernandez & Lopez, 2020). However, despite the rapid emergence of *AIT* and the subsequent *DNN*-based *UQ* (e.g., Krzywinski & Altman, 2013; Gal & Ghahramani, 2016; Zhu et al., 2019), the performance of these methods may suffer from a series of shortcomings, such as complexities arising from topology and hyperparameter choices (Asheghi et al., 2020), computational cost for multiple trainings, and weak performance due to model instabilities (Foong et al., 2019). Moreover, because *DNNs* tend to produce overconfident predictions, accurate outcome, especially in out-of-domain data, is an important issue (Loquerico et al., 2020; Klotz et al., 2021). Moreover, current *DNN*-based methods of *UQ*, such as Monte Carlo dropout (*MCD*) (Gal & Ghahramani, 2016) or quantile regression (*QR*) (Weerts et al., 2011), behave differently at training and inference time due to implemented changes in topology and optimization processes.

When using the *MCD*, *UQ* is performed through a set of trained topologies, which are subjected to randomly removed neurons, while in the *QR, UQ* is based on a conditional quantile of a dependent variable without assuming any specific conditional distribution. However, these methods typically ignore prior knowledge about the data and consequently tend to make assumptions that lead to oversimplification and thus underestimate uncertainty (Waldmann, 2018). Such concerns imply that developing new schemes or approaches to present robust *UQ* is still a crucial challenge with a tremendous potential for application in complex geo-engineering problems, particularly for *GWT* pattern modeling.

In Sweden, the *GWT* is an important part of sustainable ecosystems and for human water consumption. However, the *GWT* pattern can be affected by geo-engineering projects in combination with changes in the natural variability and the climate. Due to the significant benefits offered by an adequately accurate predictive model and the approved efficiency of *AIT* in providing more precise solution than many simulation processes, this paper addresses and then examines a new approach of systematic analysis for *UQ* through the development of an automated procedure.

Therefore, a novel state-of-the-art ensemble automated random deactivating connective weights approach (*ARDCW*) is proposed herein. In this framework, instead of dropping neurons, the connective weights between layers of the identified optimum topology are deactivated randomly. To overcome the problem of overfitting and to avoid being trapped in local minima, the *ARDCW* uses several embedded internal and nested loops to monitor all the topologies based on different hyperparameters. This approach was then applied experimentally to 244 sets of *GWT* geolocation data in an urbanized area of Stockholm. Due to the use of the optimum topology, *ARDCW* led to a state-of-the-art performance of *UQ* whereby the produced multiple predictions can be interpreted in terms of average errors. In comparison to other methodologies such as *MCD* and *QR*, the evaluated and compared performance of *ARDCW* showed superior capability in the spatial prediction of *GWT*.

STUDY AREA AND DATA SOURCE

The study area, which contained 357 investigated *GWT* wells, encompasses 20 km of an ongoing highway project in south Stockholm, Sweden. Among the monitored *GWT* data, 244 points were screened and compiled from continuous recorded intervals from 19 to 25 September 2020. The location of the study area with respect to the generated long-term map of spatial monitored *GWTs* for the entirety of Sweden is presented in Figure 2a, which was retrieved from Geological Survey of Sweden. As shown in Figure 2b, in the northwest of the study area, Mälaren Lake controls the *GWT* toward the downstream, while the coverage in the northeast consists of bedrock outcrop incorporated with intermediate soil-filled valleys. This implies that the topographical variation in the surface of the bedrock dominantly controls the groundwater flows. The *GWT* in the high terrain Masmo hills, located in the middle of the study area (Fig. 2b), mostly follows the surface topography, but without connecting to any nearby aquifers. To the southwest (Fig. 2b), homogenous bedrock and a uniform *GWT* pattern can be observed. However, in the southeast of study area, the bedrock is highly heterogenic without uniform *GWT* levels due to the influence of cracking on hydraulic connectivity. An integrated spatial distribution of groundwater aquifers with the *GWT* data over the entire study area is presented in Figure 2c.

A SUMMARY OF *UQ* ANALYSIS USING *AIT*

UQ, as one of the main challenges in *AIT*, needs extensive exploration. However, currently, the focus is often on giving a best estimate as defined by a loss function. Referring to Figure 1, Bayesian techniques (MacKay, 1992) are the main *AIT*-based framework for *UQ*. However, they are often computationally slow and difficult to train because they are traditionally formalized through parametric probability distributions of network activations and weights (Hernandez-Lobato & Adams, 2015). Sampling technique (Gal & Ghahramani, 2016) is another method used for *UQ*, but due to inability, explicitly modeling generates overconfident predictions (Hernandez & Lopez, 2020). Because an input with large noise provides wider model uncertainty than the same input with lower noise, the risk of underestimated uncertainties is increased because sampling-based methods generally disregard the relationship between data and model uncertainty (Bárdossy & Fodor, 2001; Gal & Ghahramani, 2016; Kabir et al., 2018).

Despite the significant performance of the Markov chain Monte Carlo (*MCMC*) in *UQ*, it is mostly appropriate for small networks and thus computationally expensive for large *DNNs* (Quinonero-Candela et al., 2006). However, this shortcoming can be overcome using stochastic gradient *MCMC* (Chen et al., 2014), which only needs to estimate the gradient on small sets of mini batches. Because *MCMC* requires a significant amount of time to converge on a desired distribution, the sufficient number of iterations is unknown (Neal, 2012).

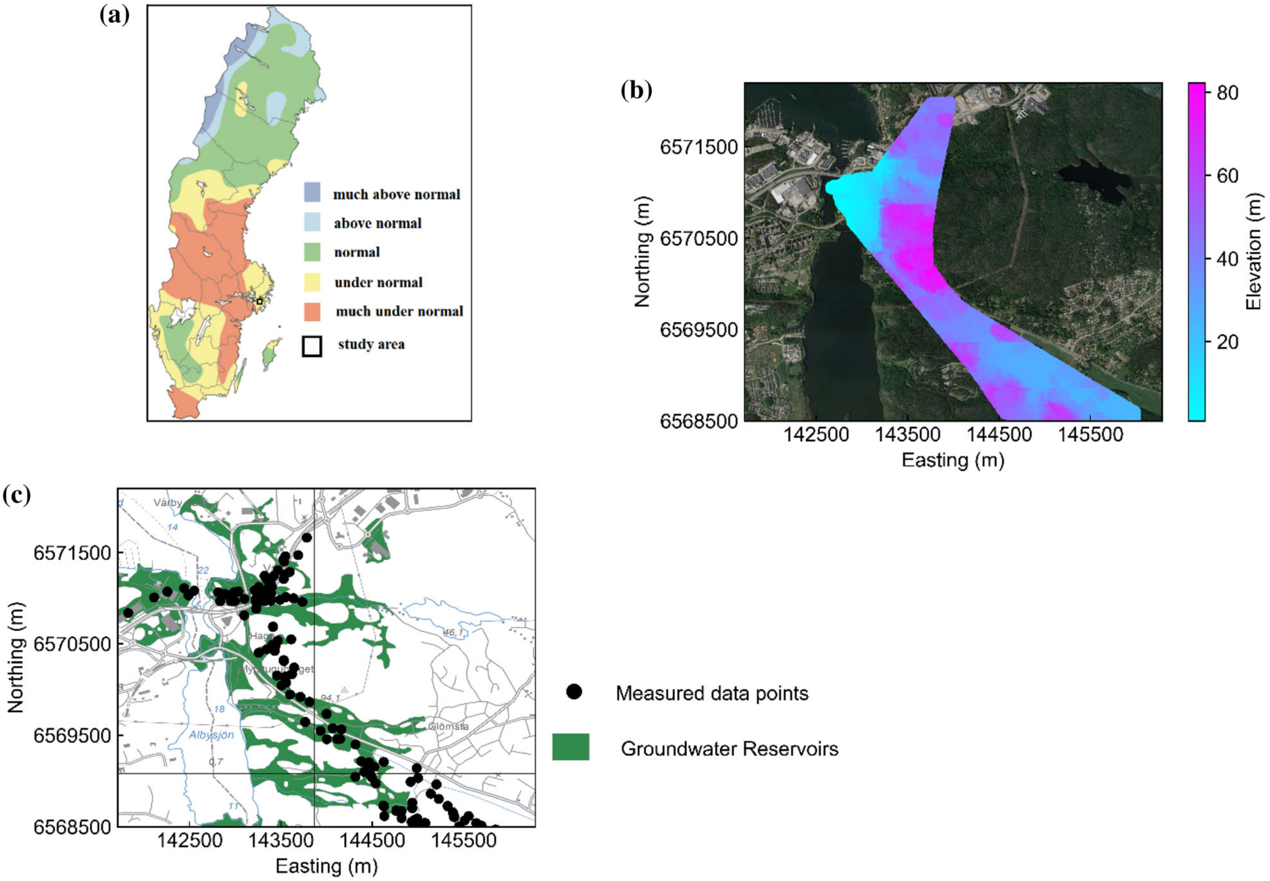

Figure 2. (**a**) Distribution of *GWT* in Sweden. (**b**) Digital elevation map overlaid on a satellite image of the study area. **c** Mapped aquifers and monitored *GWT* data in the area. (**a**) and (**c**) were retrieved from Geological Survey of Sweden.

Therefore, to provide a relatively faster approximate Bayesian solution, different methods such as variational inferences, assumed density filtering, expectation propagation and the stochastic gradient Langevin diffusion technique have been introduced (Lakshminarayanan et al., 2017). However, the posterior *UQ* in the variational method is typically underestimated rather than overestimated in the expectation propagation technique.

QR is a type of powerful regression analysis that estimates the conditional median (or other quantiles) of the response predicted values, where the quantile itself is a parameter for the loss function. This implies that for each quantile, the training process should be analyzed through individual asymmetric weighting (Yang et al., 2016). Accordingly, a trained model, when subjected to different quantiles, generates different bounds that picks out the conditional quantiles away from the median, that is, the 95% prediction intervals can be found when subjected to the quantiles 0.025 and 0.975. The mean square error, as the most commonly used loss function, would then correspond to the Gaussian distribution. Accordingly, the mode (peak) of this distribution corresponds to the mean parameter, and *DNNs* predict the mean value of the output, which may have been noisy in the training set. Moreover, the dependency of the quality of prediction on computational complexity, degree of approximation and correctness of the prior distribution implies that *UQ* using these methods cannot be guaranteed to provide underlying beliefs (Hirschefeld et al., 2020).

UQ can be performed using ensemble-based methods, whereby inputs are trained and passed through multiple networks (Fig. 3a). Greater accuracy can be achieved by using such methods than any individual model because the predictions vary across multiple runs of a set of models $M = \{M_1, M_2,$

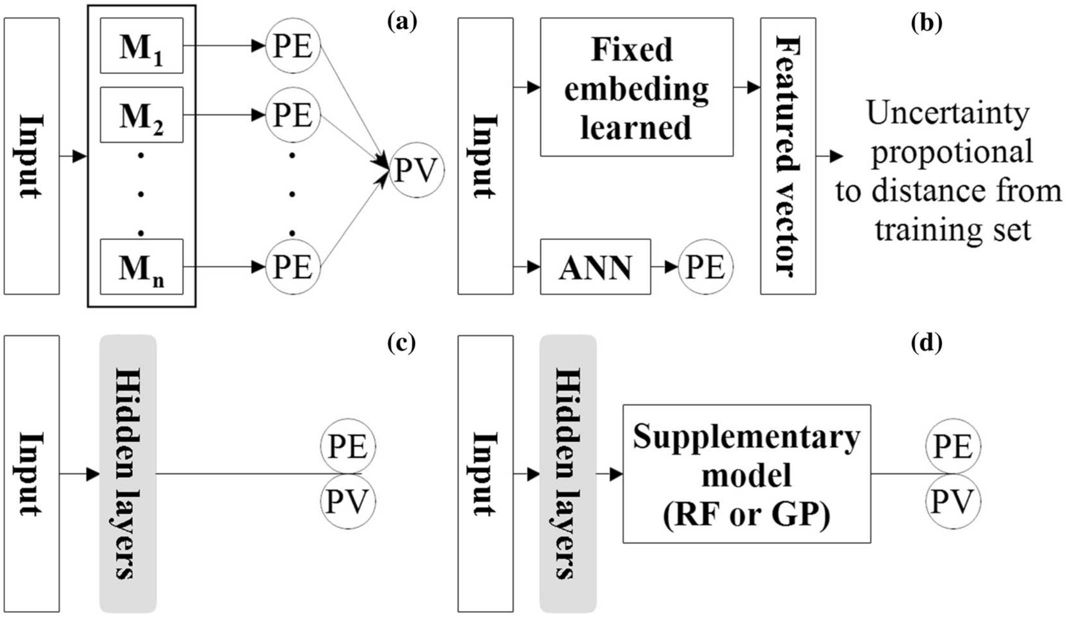

Figure 3. Simplified schematic of different strategies for *UQ*: (**a**) ensemble-based, (**b**) distance-based, (**c**) mean variance and (**d**) union-based. *PE* = predicted error. *PV* = predicted variance.

…, M_n} rather than training a single M_i. However, the primary drawback of any ensemble-based method of *UQ* is the increased training time, depending on the size of the ensembles. As presented in Figure 3, in addition to ensemble methods, the *UQ* can be based on mean–variance, distance-based strategies and union-based strategies (Angiulli & Fassetti, 2020; Hirschefeld et al., 2020; Zhang et al., 2020). The problem with training Bayesian neural networks for large data sets can be solved by using mean–variance estimation, where the output layer is modified and trained using a negative log likelihood loss to predict both the mean and variance of the interested input (Hirschefeld et al., 2020). Through distance-based methods, the minimum distance between each interested prediction from its nearest neighbors in the training set is interpreted as uncertainty. The larger the distance between the training sets and predictions, the higher the error and thus the greater the uncertainty (Angiulli & Fassetti, 2020). However, significant sensitivity of the calculated distance to outliers is the major drawback of this estimator in *UQ*. The union-based method (Huang et al., 2015) is a combined confidence estimator, where the output of the trained neural network is fed to another model to provide an ensemble model and thus calculate uncertainty into the task-specific latent space.

The *MCD* (Gal & Ghahramani, 2016) is one of the most widely used methods for *UQ* and it can even be implemented on an already trained model. In this procedure, any trained topology with dropouts is used to prevent overfitting and can thus be interpreted as an approximate inference of the posterior weights. Accordingly, the average of multiple predictions for the analysis of distributions is considered to calculate meaningful variance. In a fixed topology during the *MCD* process, all in/out connective weights and biases of dropped neurons are ignored. This implies that in each dropout, the data are trained using a different topology, while none of these connectives participate in the prediction process nor will they be updated. Therefore, the dependency of *UQ* on the dropped neuron and internal hyperparameters is the main drawback of *MCD*. Moreover, due to the training of several topologies, the produced approximations can be categorized in ensemble techniques, which significantly enable improved overall performance (Dietterich, 2000). In comparison to the Bayesian approach (MacKay, 1992), which attempts to average and thus find the single best model (or parameters), ensembles combine the topologies to obtain a more powerful model. Therefore, ensembles potentially provide a complementary source for predictive *UQ*. Referring to Figure 4, *UQ* through the *MCD* is performed over multiple networks at the test time, where a model with *n* neuron can provide a collection of *2*^{n} possible topologies as an ensemble combination (Srivastava et al., 2014).

PROPOSED *UQ* APPROACH

In recent years, *UQ* using different *AITs* has increased because the provided models can offer simple but precise solutions in many engineering simulation problems. Systematic *UQ* can be applied by considering a combination of several components, including data, model structure and parameter values. This implies that *UQ* should be conceptualized in a concrete mathematical sense and thus be amenable for programming. Because noise will be produced in each random dropping, which will affect results, therefore, mathematically, the performance and predictability of the *DNN* structure should always be evaluated with the original optimum model. By using the dropout concept integrated with the optimum topology, the ensemble automated random deactivating connective weights (*ARDCW*) approach was proposed. The *ARDCW* is focused solely on randomly switched off weights, not neurons, where the remaining weights are forced to participate in learning processes and assist in decreasing the overfitting. Accordingly, this approach uses an optimum trained topology capable of performing a given task even when the weights are randomly sampled. This implies that the training of multiple different topologies is avoided, as the uncertainty will be estimated by changing the internal assigned weights of a fixed optimum model.

In a *DNN* topology, all *m* neurons of a layer are associated with probability *p*, otherwise they are dropped (set to zero), with probability *1- p* (Hinton et al., 2012). According to probability theory, the expected value of a random variable (*E[X]*) is a generalization of the weighted average with probabilities of p_i as:

$$E[X] = \sum_{i=1}^{n} x_i p_i \text{ where } \sum_{i=1}^{n} p_i = 1 \tag{1}$$

Mathematically, for a constant random variable, $E[X = c] = c$. Therefore, $E[X]$ with equiprobable outcomes $\{c_1, c_2, \ldots, c_n\}$ expresses the arithmetic mean of the terms with probabilities $P(X = c_i)$. Using this concept, the impact of dropped weights ($\hat{w}_{\mathrm{ij}}$) in *UQ* can be described with mean field theory (Kadanoff, 2009) as:

$$\hat{w}_{ij} = \begin{cases} w_{ij} \text{ with } p(c) \\ 0 \text{ otherwise} \end{cases} \tag{2}$$

where $P(c)$ denotes the probability of keeping a weight, whereby the implemented neurons are kept with the probability *p* and otherwise will drop (0) with probability *1-p*. This implies that the *UQ* can be generalized by dropping the connective weights with probability *1-p* rather than the neurons (Wan et al., 2013). Consequently, in a topology with *h* hidden layers, where $Z^{(l)}$ and $y^{(l)}$ denote the vector of inputs into and output from layer l ε {1, 2, …, *h*}, the feed-forward process is described as:

$$z_i^{(l+1)} = w_i^{(l+1)} y^l + b_i^{(l+1)} \tag{3}$$

$$y_i^{(l+1)} = f\left(z_i^{(l+1)}\right) \tag{4}$$

where $w_i^{(l+1)}$, $b_i^{(l+1)}$ and *f* denote the weight, bias and applied activation function, respectively. Referring to neural network topology, the activity of dropout weight of the *i*th neuron in *h*th hidden layer (a_i^h), and consequently the corresponding output (O_i^h), can be expressed as:

$$a_i^h = \sum_{l<h} \sum\nolimits_j w_{ij}^{hl} \delta_{ij}^l a_j^l \text{ with } a_j^0 = X_j \tag{5}$$

$$O_i^h = f\left(a_i^h\right) = f\left(\sum_{X<h} \sum\nolimits_j w_{ij}^{hl} \delta_{ij}^l a_j^l\right) \text{ with } O_j^0 = X_j \tag{6}$$

where δ_{ij}^l is a gating 0-1 Bernoulli variable with $P(\delta_{ij}^l{=}1) = \ p_j^l$. Therefore, in dropout, the output of layer *l* using element-wise product (*) is then presented as:

$$z_i^{(l+1)} = w_i^{(l+1)} \left(p_i^l * y^l\right) + b_i^{(l+1)} \tag{7}$$

Accordingly, the expectation of the activity of all neurons for a fixed input vector taken over all possible δ_{ij}^l variables, and thus the possible ensemble models, can be achieved as:

$$E\left(a_i^h\right) = \sum_{l<h} \sum\nolimits_j w_{ij}^{hl} p_j^l E\left(a_j^l\right) \text{ for } h>0 \tag{8}$$

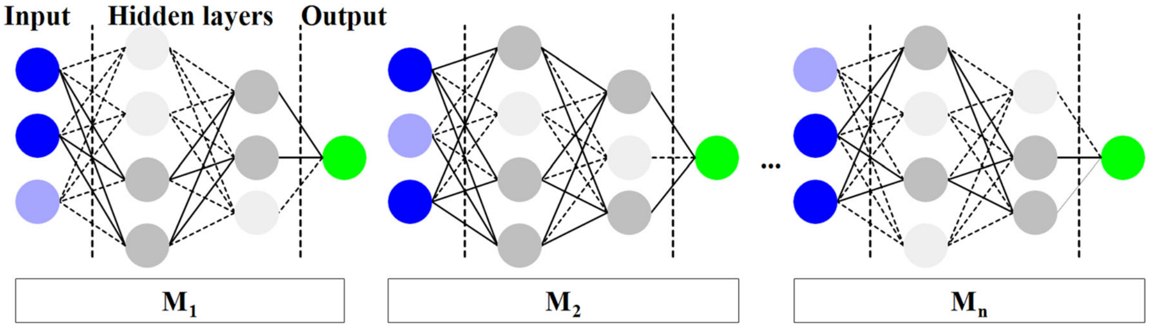

Figure 4. Overview of *MCD* modeling process mimicking ensemble-based method (highlighted and dash lines correspond to dropped neurons and weights).

The dropout is not applied on a fixed input that produces a constant output in the lth layer (O_j^l); thus, the dropout on the hth hidden layer is then presented as:

$$Var\left(a_i^h\right)=\sum_{l<h}\left(w_{ij}^{hl}\right)^2\left(O_j^l\right)^2p_j^l(1-p_j^l) \qquad (9)$$

where *Var* is the variance. Therefore, the expectation of dropout gradient as a random variable is the regularized ensemble error associated with all possible models (E_{ens}) and is expressed as:

$$E\left(\frac{\partial E_D}{\partial w_i}\right)=\overbrace{\frac{\partial(0.5(t-\sum_{i=1}^n p_iw_iX_i)^2)}{\partial w_i}}^{\text{regularized } E_{\text{ens}}}+w_ip_i(1-p_i)X_i^2\overbrace{\frac{\partial(0.5(t-\sum_{i=1}^n p_iw_iX_i)^2)}{\partial w_i}}^{\text{regularized } E_{\text{ens}}}+w_iX_i^2Var(\delta_i) \qquad (10)$$

$$E[\text{dropoutgradient}]=E_{ens}+0.5\sum_{i=1}^n w_i^2X_i^2Var(\delta_i) \qquad (11)$$

where t is the target value of input X_j and E_D denotes the error of the network with dropout. With recourse to Eqs. 8 and 11, additional layers corresponding to real-valued output for error or variance can be attached to the optimum topology. This implies producing a multi-objective model, where the output of error and variance are also predicted using the same fixed optimum *DNN* with an added layer(s).

Referring to presented block procedure of the proposed *ARDCW* (Fig. 5), it does not require any changes in optimum topology and thus can even be used for already trained models. In this process, the optimum topology was captured through the proposed automated strategy by Abbaszadeh et al. (2021b). The performance of the optimum model is then monitored through the randomly sampled deactivated weights using an automated dropout procedure for the achieved database. Since all deactivations occur for the one optimum topology, the *ARDCW* captures different models and, as shown in Figure 3a, it can be interpreted as an ensemble-based Bayesian approximation of the Gaussian process probabilistic model. Accordingly, the inadvertent tuning on the model is addressed through a regularization strategy, which needs a robust implementation that accounts for floating-point stability and reproducibility in geo-engineering-related problems. The minimum number of sampled weights in this study is 1, while the maximum number of desired droppings was set at 50% of the whole connective weights. Although selecting this rate for dropout is flexible and user defined, the dependency on the topology and network type (shallow or deep) that overfits the training data should be considered. Moreover, the greater the number of deactivations, the more examined ensembles, which thus requires more analysis time.

As an advantage, in each examination, the model is trained using a constant topology but with a different set of randomly deactivated weights in the layers. Therefore, the outcome can be considered as an averaging ensemble of many different models trained on one batch of data only. The *ARDCW* can be regularized to calculate the mean and variance of randomized data and can then predict unlabeled

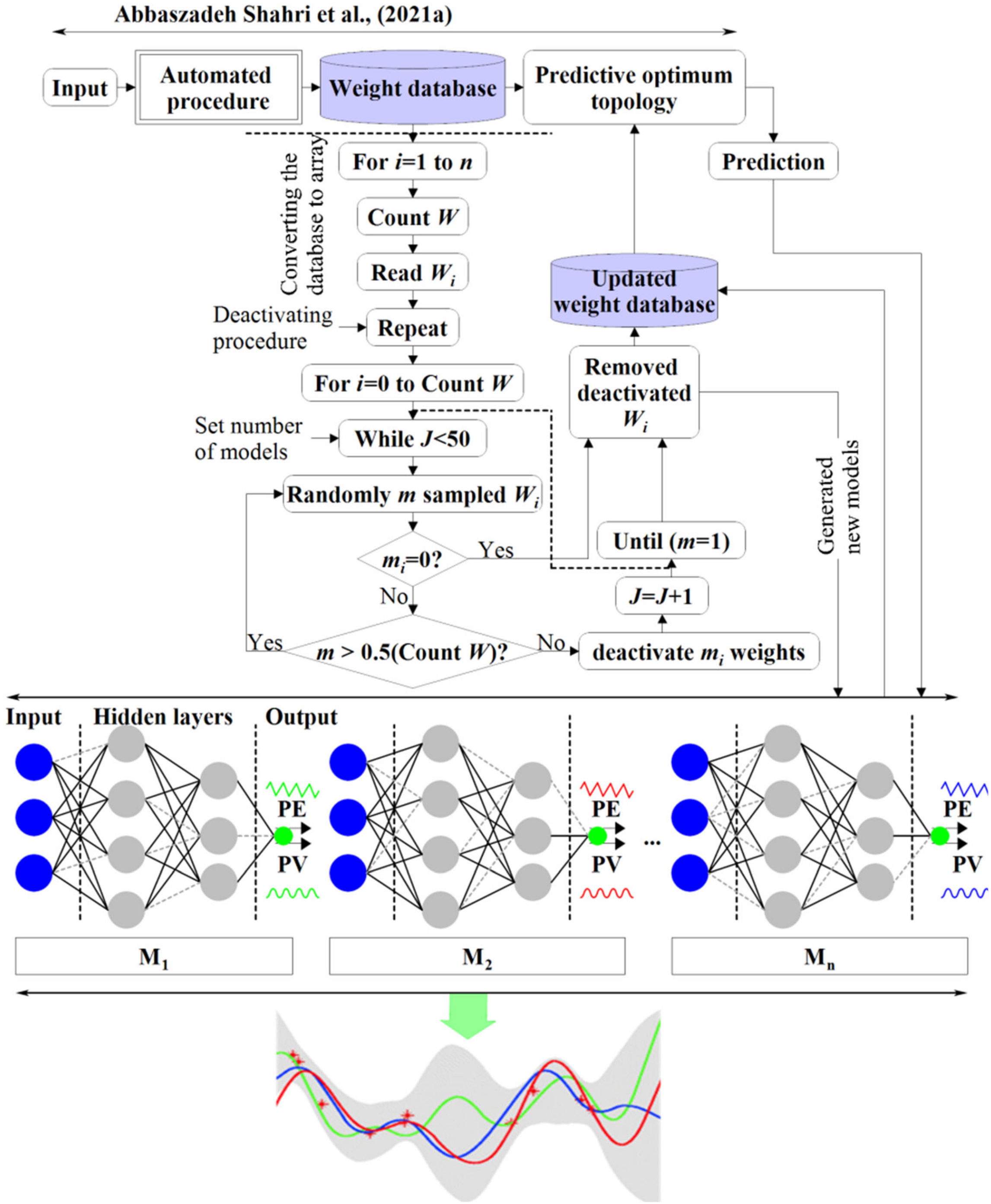

Figure 5. Block diagram of the proposed *ARDCW* approach for *UQ* modeling (n: number of weights, W_i: weight components, J: number of models, m: number of randomly sampled weights).

data. Moreover, using the optimum model will minimize the problem of overfitting, while the overall performance of the *DNN* topology due to randomly switched off weights in each layer becomes less sensitive.

RESULTS OF EXPERIMENTAL APPLICATION

The randomization process increases the predictability skill of system in training and dedicate more generalize findings. It then leads to more powerful developed predictive systems in evaluating the unseen data. This implies that, through random shuffling, the chances of last few batches being disproportionately noisy will reduce. Because there are no special rules in percentage of randomizations, 65, 20 and 15% for training, testing and validation were used (e.g., Xu & Goodacre, 2018; Ghaderi et al., 2019). In configuring the optimum model, the regularization and tuning of hyperparameters (e.g., training algorithm, number neurons, layer arrangements, learning rate, activation function and architecture) played a significant rule to overcome trapping in local minima, overfitting and early convergence. Therefore, the automated approach proposed by Abbaszadeh et al. (2021a) as presented in Figure 5 was employed to capture the optimum model. This system using several inner nested loops integrated with constructive technique can automatically monitor the different combinations of hyperparameters and thus provide faster learning procedure. According to Figure 5, by applying 65% of the 244 compiled *GWT* data, a 3-32-8 topology subjected to hyperbolic tangent activation function trained with quasi-Newton algorithm was considered as the optimum, which was then retrained using two extra predicted outputs, including the error and variance. Considering the y and $\hat{y}$ as the target and model output, respectively, the error and variance were predicted through $(y - \hat{y})$ and $(y - \hat{y})^2$. Referring to Figure 4, a series of models was retrained using the updated dropout weights database (Fig. 5) subjected to the fixed defined custom loss function in optimum topology for each mini batch. To visualize the range of predicted distribution, the results of the randomly deactivated weight using *K*-fold validation for a series of dropout test sets are presented in Figures 6 and 7. Accordingly, Figure 6a shows the variation of the predicted *GWT* from all the K-fold validations using *ARDCW*, and uncertainties at each point can be estimated from these outcomes. Subsequently, the errors between the observed and predicted *GWT* in each *K*-fold validation are reflected in Figure 6b, which shows high error values and thus high uncertainties at data points. Figure 6c depicts the variance of errors as described where uncertainties are high. According to these outcomes, *PE* and *PV* derived from *UQ,* when subjected to different random dropouts are more preferred due to lower variance estimators. Proper experimental measurement associated with an estimated level of confidence not only allows a scientific hypothesis to be confirmed or refuted, but also facilitates the judgments on the quality of the data and leads to meaningful comparisons with other similar values or predictive models. Accordingly, 95% prediction interval (*PI*), which is often used in regression analysis, shows the certain probability of an estimation of future observation (Fig. 8).

Due to the dynamic nature of areas without data, creating a 3D visual perspective depicting the predictive spatial distribution of the *GWT* levels is a challenging task, but this can provide more utility in interpreting the subsurface characterization (Abbaszadeh et al., 2020, 2021a). However, the level of accuracy and the confidence of the model can vary depending on the quality of available data and the approach. This is the reason why pseudo data can therefore play an important role in building knowledge for unsampled locations (Tacher et al., 2006; Cruzes & Dyba, 2011; Abbaszadeh Shahri et al., 2020). Figure 9 shows the step-by-step creation of the 3D model of the study area depicting the retrieved outlines of the uncertainties. In this process, the produced digital elevation model of the area (Fig. 9a) was incorporated with the 3D spatial distribution of acquired *GWT* (Fig. 9b) and corresponding results of the automated predictive optimum topology (Fig. 9c). The estimated uncertainties of the optimum topology in the level of 95% using the proposed *ARDCW* were then added (Fig. 9d, e). Referring to the estimated uncertainties, more comprehensive spatial *GWT* patterns can be realized to avoid the relevant risk of facing aquifers during geo-engineering projects. Due to the ease of updating with new data, the flexibility of such models provides a preferred tool for geo-engineers and decision planners in the observation and analysis of geo-environmental engineering issues within a project.

DISCUSSION AND VALIDATION

Predictive *AIT*-based models are indispensable tools in geo-engineering applications, not only to ensure the function in labeled variables but also to estimate uncertainty in unlabeled data. In recent years, several studies have been dedicated to the

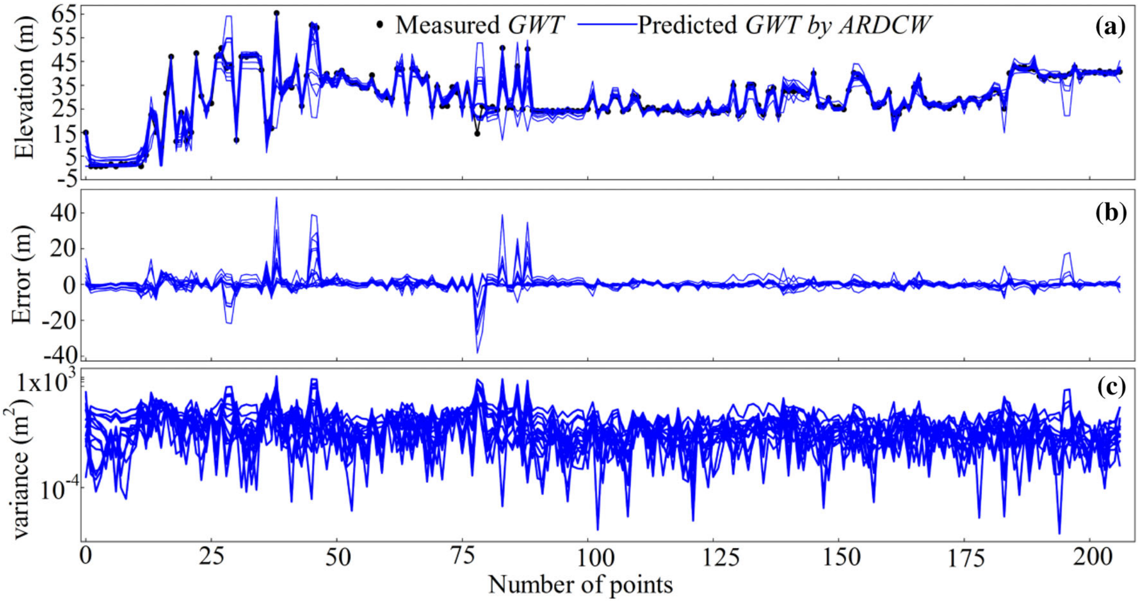

Figure 6. Predictability of the optimum model subjected to applied dropouts in training and testing stages for *GWT* (**a**) data, (**b**) mean and (**c**) variance.

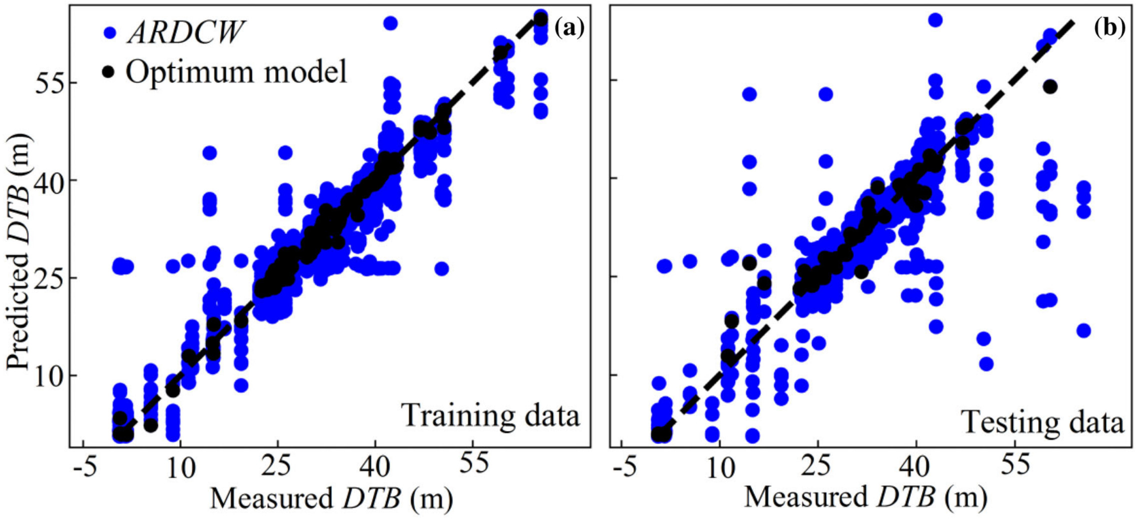

Figure 7. Comparison of distributions of optimum and dropout models for (**a**) training and (**b**) testing data sets.

importance of *UQ* in *GWT* modeling and decision-making at different scales (WWAP, 2012; Middlemis & Peeters, 2018). However, from geo-engineering point of view, each parameter of a geologic object can be a source of uncertainty and, thus, in practice, the number of involved sources can be innumerable. To evaluate the robustness and accuracy of the predictive spatial pattern of *GWT*, *UQ* is often required. Because standard *AIT*-based procedures of *UQ* are still limited, developing an efficient method that uses *DNN* predictive models in particular is of great interest for industrial-scale and real-world applications. In the current paper, the presented *UQ* approach, *ARDCW*, is discussed and validated using contour maps of predicted error in different dropouts, accuracy metrics and success rate, and by comparison with *MCD* and *QR*.

Effects of Dropout on Estimated Uncertainty

This concern was monitored by comparing variations of captured distributions in post and prior predictions with respect to the optimum topology. These variations are referred to in the *ARDCW* by using the saved updated database for each examined model (Fig. 5). The comparison of different post distributions and the corresponding residual contour map of the area are given in Figure 10 to show how the dropped weights can influence on the variation of the captured functions in the optimum topology. Therefore, the uncertainty of the optimum model can be evaluated through the sampled weights, where each plot depicts a single draw from the prior functions. Accordingly, multiple repetition of *ARDCW* can inspire an idea of the prior functions and weight matrices over the fed inputs, which help to find a function to fit variational objective data with the minimum penalty with respect to the prior distribution in the optimum model. This implies that in case of a lack of observations, the uncertainty can be interpreted through the interpolation of unlabeled predictions.

Figure 9. Incorporating results of predictive optimum topology and the proposed *ARDCW* in visualizing the estimated uncertainty: (**a**) surface of the area, (**b**) measured *GWT*, (**c**) predicted *GWT*, (**d**) upper and lower limits of estimated uncertainties, and (**e**) overlay of supplementary perspective for the entire study area.

Uncertainty is generally evaluated from data and models due to the presence of noise and an imbalanced training data distribution (Loquerico et al., 2020). In *AIT*-based models, the source of uncertainty occurs when the feed data are mismatched, where smaller differences between the observed *GWT* and those predicted by *ARDCW* show a higher degree of safety in the prediction process (Fig. 11a, b). Subsequently, stronger differences can be interpreted as higher uncertainties in prediction. Accordingly, the performance of the optimum and examined *GWT* models using *ARDCW*, as well as error for the measured and unlabeled prediction datasets, are given in Figure 11c and d.

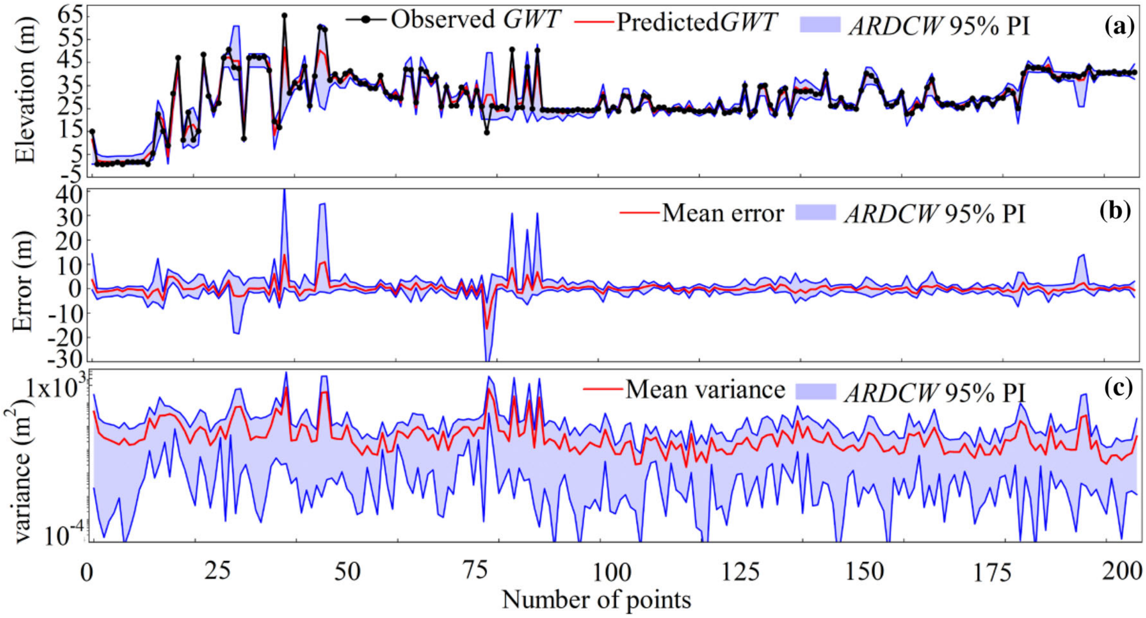

Figure 8. Calculated *PI* using the optimum model for *GWT* (**a**) data, (**b**) predicted mean and (**c**) predicted variance.

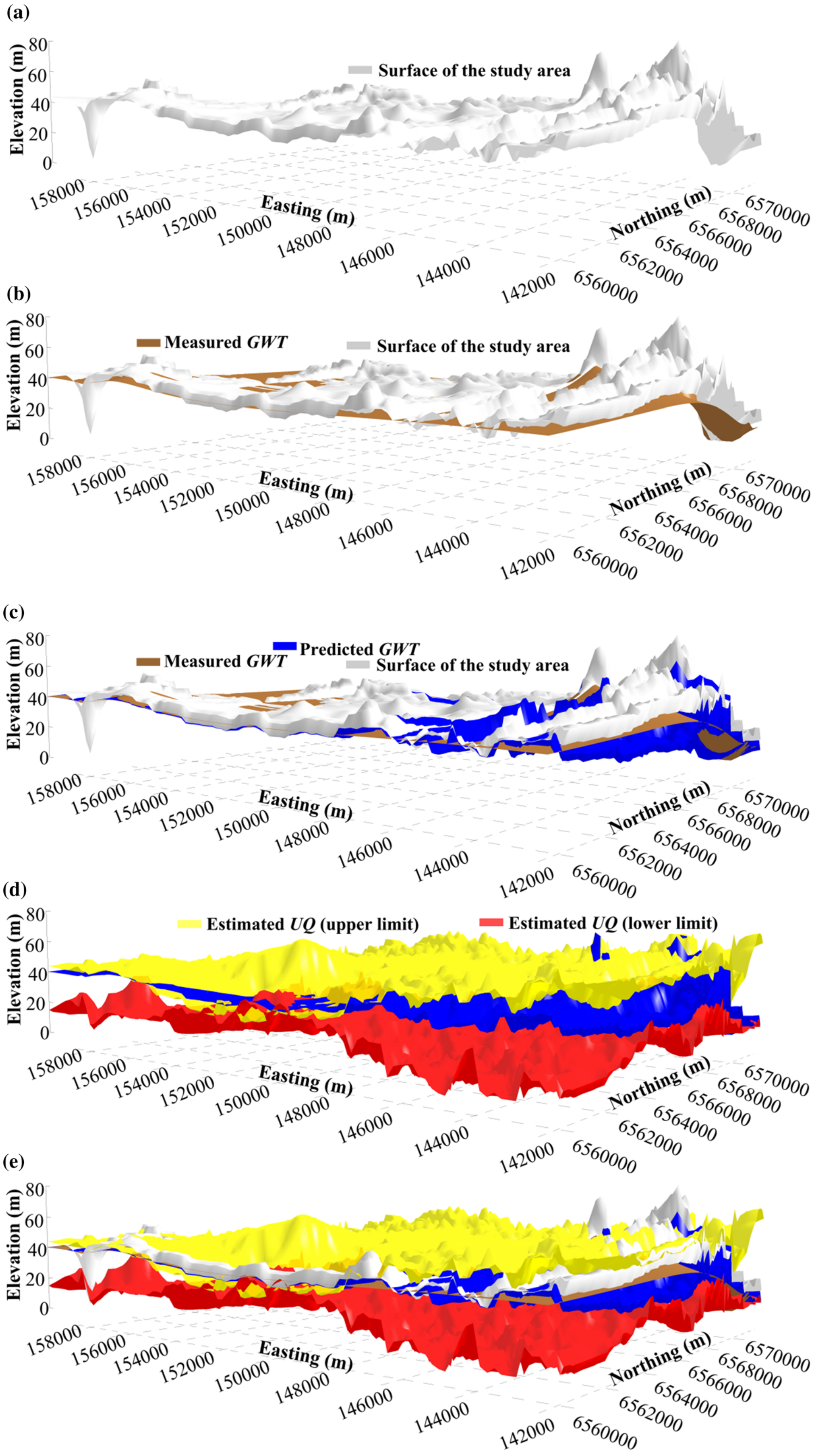
(a)
Elevation (m)
80
60
40
20
0
Surface of the study area
158000
156000
154000
152000
150000
148000
146000
144000
142000
Easting (m)
Northing (m)
6560000
6562000
6564000
6566000
6568000
6570000
(b)
Measured GWT
Surface of the study area
(c)
Predicted GWT
Measured GWT
Surface of the study area
(d)
Estimated UQ (upper limit)
Estimated UQ (lower limit)
(e)

Comparing Different Uncertainty Models

Statistical Metrics

The coefficient of efficiency (*Ec*) (Nash & Sutcliffe, 1970) is one of the most widely used metrics for evaluating the performance of hydrologic models, thus:

$$E_c = 1.0 - \frac{\sum_{i=1}^{N} (O_i - P_i)^2}{\sum_{i=1}^{N} \left(O_i - \overline{O}\right)^2} \quad \overline{O} : \text{observedmean} \tag{12}$$

where N is the total number of *GWT* data, O_i and P_i denote observed and predicted data, $E_c\varepsilon$ is interval $(-\infty, 1.0]$ in which the value of 1.0 expresses perfect fit. $E_c = 0$ reflects large variability in the observed data, while $E_c < 0$ indicates that the $\overline{O}$ would have been a better predictor than the model. Further, E_c is the ratio of mean square error (*MSE*), thus:

$$MSE = N^{-1} \sum_{i=1}^{N} (O_i - P_i)^2 \tag{13}$$

Therefore, E_c represents an improvement over the coefficient of determination for model evaluation purposes in that it is sensitive to differences in the observed and model simulated means and variance (Leavesley et al., 1983; Wilcox et al., 1990).

To cover the lack and insensitivity of E_c and R^2 in considering the calculated square differences between the observed and predicted means and variances (Legates & McCabe, 1999), the index of agreement (Willmott, 1984), which is the ratio of mean square and potential errors is defined as:

$$IA = 1 - \frac{\sum_{i=1}^{N} (O_i - P_i)^2}{\sum_{i=1}^{N} \left(\left|P_i - \overline{O}\right| - \left|P_i - \overline{O}\right|\right)^2} \tag{14}$$

The percentage of observed *GWT* (N_{GWT}) bracketed by confidence interval (*CI*) in the 95% level ($P_{CI}^{95\%}$) is defined as:

$$P_{CI}^{95\%} = \frac{N_{GWT}}{N} \times 100 \tag{15}$$

whereby the properly modeled uncertainty is justified based on the closeness to 100%.

Referring to Jin et al. (2010), the quality of the predicted uncertainty can be assessed using the average relative interval of the *CI* (*ARIL*), thus:

$$ARIL_{CI}^{\%95} = \frac{1}{n} \sum_{i}^{n} \frac{UCL_{pred,i}^{GWT} - LCL_{pred,i}^{GWT}}{GWT_i^{obs}} \tag{16}$$

where $UCL_{pred,i}^{GWT}$ and $LCL_{pred,i}^{GWT}$ express the calculated upper and lower *CI* of the *i*th predicted *GWT*, and n is the number of total observations; thus, a lower $ARIL_{CI}^{\%95}$ value represents better performance.

A comparison of the above indices in evaluating the predicted uncertainty using three different methods, namely *ARDCW*, *QR* and *MCD*, is given in Figure 12 and Table 1. Referring to $P_{CI}^{95\%}$, although both *ARDCW* and *QR* showed competitive coverages of the true *GWT* levels (95%) with respect to *MCD* (68%), the ranking score of *ARDCW* was superior to those of the other methods. The closeness statistics of the *ARDCW* and *QR* methods can be interpreted as similar properties of posterior distribution of predicted *GWT* for these methods.

Success Rate Using Confusion Matrix

A confusion matrix can intuitively describe the performance of a model based on a set of data using the true labeled instances (Asheghi et al., 2019). This concept conceptualizes the error probabilities of developed models in assigning the individual predicted outputs into the classified input. The best performance is defined by zeroes, except on diagonals. Referring to obtained confusion matrix (Table 2), *ARDCW* and *QR* methods provide more true predicted instances (33 and 29 out of 37) compared to *MCD*. As presented in Table 3, the performance of *ARDCW* in terms of classification accuracy and misclassification error at an 89% correct classification showed 22 and 14% improvement in estimated uncertainty over those by *MCD* and *QR*, respectively.

Uncertainty Intervals in Studied Area

Sufficiently accurate modeling procedures are essential tools in subsurface geo-engineering disciplines to reflect fidelity between the real and counterparts. However, despite enhanced computational power, different sources such as modeling errors in describing the real system, numerical errors generated by mathematical equations, and data errors caused by uncertainties can cause the appearance of

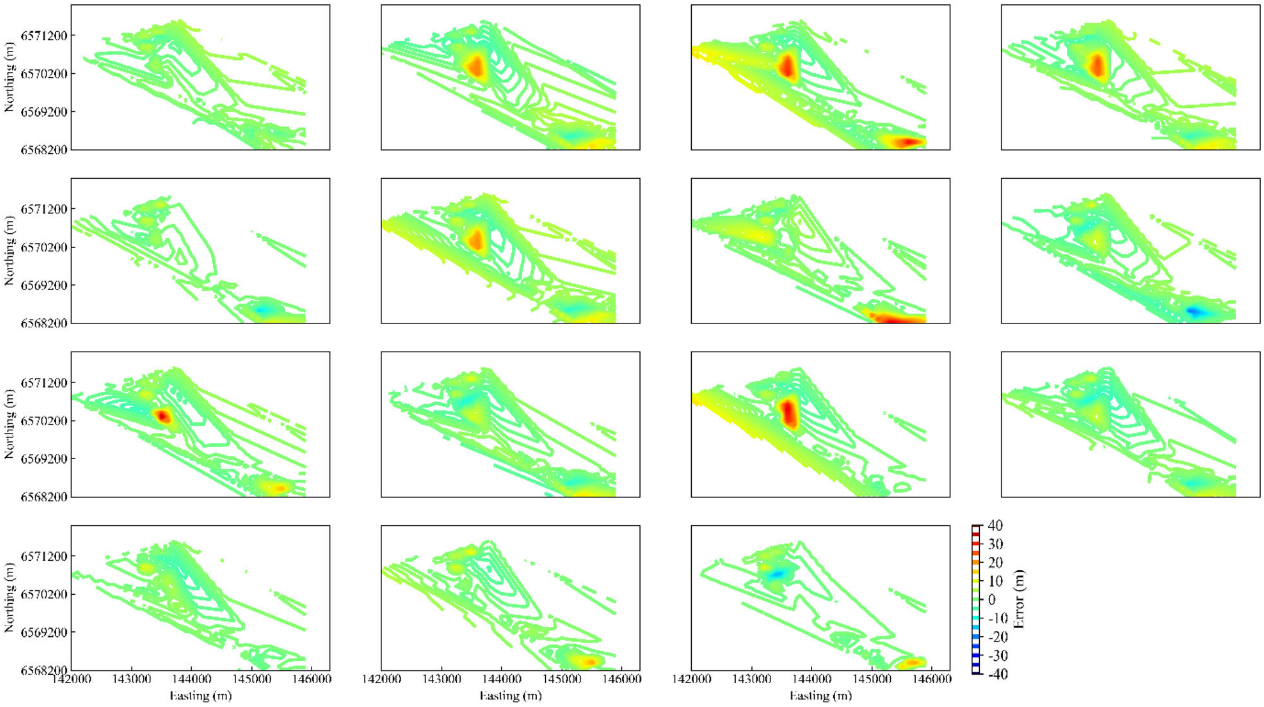

Figure 10. Contour maps of residuals for different results of *ARDCW*.

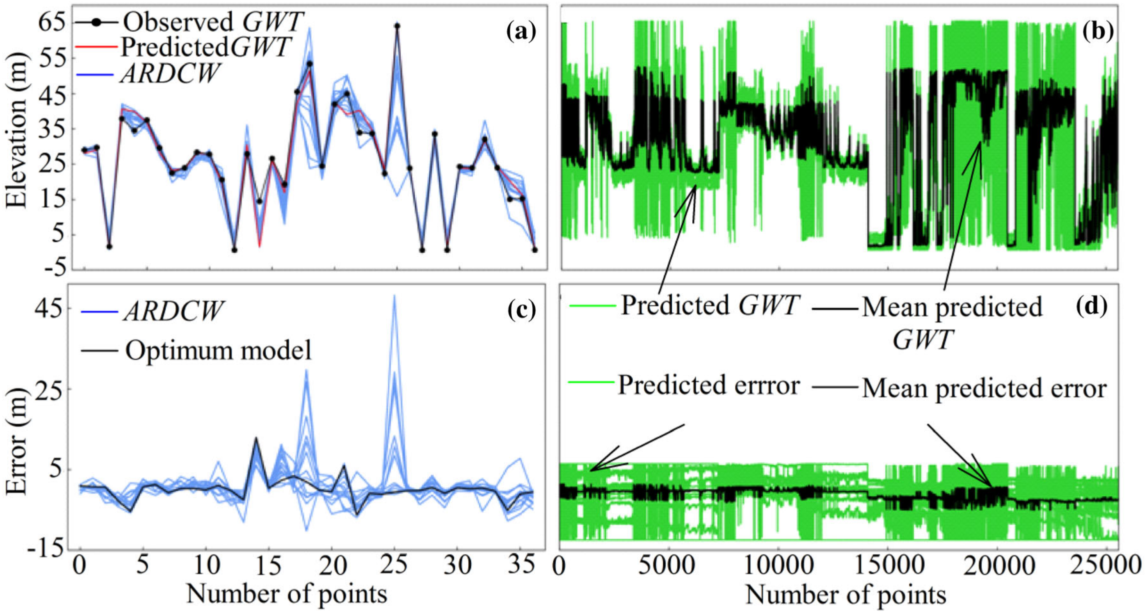

Figure 11. Variations of predicted *GWT* and error for (**a**), (**c**) validation data and (**b**), (**d**) unlabeled data.

Table 1. Comparison and rankings of the *UQ* models through statistical metrics

Model	Performance criteria							Ranking of criteria								
	E_c	*RMSE*	*IA*	R^2	$P_{CI}^{95\%}$	$ARIL_{CI}^{\%95}$	$P_{PI}^{95\%}$	E_c	*RMSE*	*IA*	R^2	$P_{CI}^{95\%}$	$ARIL_{CI}^{\%95}$	$P_{PI}^{95\%}$	Total rank	Sort order
ARDCW	0.97	2.51	0.99	0.97	10.66	3.52	0.95	3	3	3	3	1	2	3	18	1
QR	0.96	2.99	0.99	0.96	10.44	2.73	0.95	2	2	3	2	2	3	3	17	2
MCD	0.94	3.5	0.98	0.94	9.5	5.76	0.68	1	1	1	1	3	1	1	9	3

differences. A critical part of prediction is assessment of how much a predicted value will fluctuate due to noise or variations in the data. Figure 13 shows the 95% uncertainty intervals estimated using *ARDCW* for the studied area. It can provide the distribution of different uncertainty levels and it gives an indication of the reason for high uncertainties; for example, if uncertainty arises from lack of observed data or from sudden big changes in the groundwater levels. This map can also help in the planning of future data collection and determining where to drill more groundwater boreholes to reduce high uncertainties in estimating the groundwater surface.

Comparison of CI and PI

Due to the dynamic nature and time-dependent behavior, the exact modeling of *GWT* problems is a complex issue to resolve. The time-dependent *GWT* data points over an interval can benefit from outlier removal to present an overall perspective of variation in the study area as well as a better analysis and understanding and thus uncover patterns in datasets for future forecasting (Shumway, 1988; Keogh & Kasetty, 2003). However, the problems regarding generalization from a single study, difficulty in obtaining appropriate measures, and accurately identifying the correct model to represent the data should be considered.

Therefore, the bias and discrepancy of the applied models can be interpreted through comparison of the estimated uncertainty. Statistically, a predictive model is stable and under control if most of the predictions fall within the range of the *CI*. This range refers to the long-term success rate of the method in capturing the predicted output, whereby the wider the *CI*, the greater the instability. The *CI* level of 95% reflects a range of values where 5% can contain the false mean of the population. Due to lack of knowledge, observation error (variability of experimental measurements) and the underlying physics in *GWT* problems, such a comparison (Fig. 14) can show how accurately a mathematical model describes the true system in a real-life situation. Mathematically, the variations in predicted uncertainty come from the adjusted model parameters and, correspondingly, the implemented algorithm as well as feed input variables whose exact values are unknown or cannot be inferred by statistical methods (Kennedy & O'Hagan, 2001).

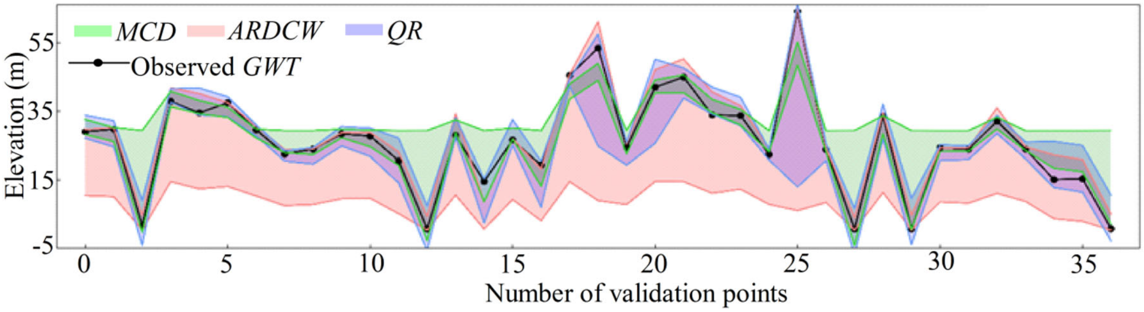

Fig. 12. Comparison of $P_{CI}^{95\%}$ of the three models based on the validation dataset.

Therefore, the dimensionality of an engineering problem would cause variability in its performance, whereby the implemented algorithm can provide discrete numerical uncertainty.

CONCLUDING REMARKS

AI-based models are becoming a standard computational and decision-making tool in civil and construction industries. However, due to inherent complexities, computational costs and poor performance, most of the *AI*-based methods of *UQ* rarely make the leap from research to production. Therefore, in this context the need for a validated coding procedure able to meet the regulatory requirements was highlighted in this paper. In order to gain insight into the predictability level of the complex *AIT*-based predictive subsurface geo-engineering model, an evaluation of the estimated uncertainty using simulation codes with iterative analyses is required. Moreover, because a model or method can be adjusted using a wide range of internal characteristics, subsequently presenting reliable but robust uncertainty estimates presents a significant challenge. Therefore, if *AI* systems could reliably identify unlabeled data, they could be deployed with a greater degree of certainty. This concern is especially vital for geo-engineering applications, where the expectation is to achieve the same distribution for observations and the training data.

In response to greater demand for *DNN*-based methods of *UQ*, the *ARDCW,* as a new state-of-the-art approach that applies randomly weighted components that dropout at test time, was introduced and developed. Using *ARDCW,* the estimated uncertainty was visualized using the average results of many ensembled predictive models derived from a demonstrated learned optimum automated *DNN* topology through *K*-fold validation and randomly deactivated weights. The issue of underestimated uncertainty, which is usually observed in most *AIT*-based methods of *UQ*, originates from changes in model and optimization process. In this point of view, the *ARDCW* approach does not require any changes in the topology and can be applied on already trained models. Because the *ARDCW* is built on a weight database, it does not have restrictions in application on time-dependent data such as *GWT* with sequences of seasonal fluctuations in monitored data over different intervals of the year. However, presenting a seasonal time-dependent *GWT* model was beyond the scope of this paper.

An experimental application of the proposed *ARDCW* was applied to 244 measured *GWTs* from a geo-engineering project in Stockholm, Sweden. The 3-32-8-1 predictive *DNN* topology, as the characterized optimum model, showed significant competence in comparison with *MCD* and *QR*. The results showed that due to the use of different topologies, the *MCD* can behave differently at training and inference time, while for assured dropout creating a custom layer with predefined training parameters for regular dropout should be employed.

Using the *ARDCW,* the estimated uncertainty boundaries with 95% level of *CI* were visualized and presented on the generated 3D predictive spatial pattern of subsurface *GWT* data. This cost-effective and adequately accurate tool can reflect the potential risks associated with the distributed spatial aquifers, thus preventing water inrush, or facing underground geo-structures. The validity of most analyzed *GWTs* with respect to both engineering and societal challenges is limited in the findings as it is often not included in uncertainty assessment. This implies that uncertainty should be estimated in

Table 2. Comparison of success rates of different *UQ* methods for *GWT* data

Target	*ARDCW*												Results		
	[< 0.62]	[0.62, 6.98]	[6.98, 13.34]	[13.34,19.70]	[19.70, 26.06]	[26.06, 32.42]	[32.42, 38.78]	[38.78, 45.14]	[45.14, 51.50]	[51.50, 57.86]	[57.86, 64.22]	[> 64.12]	Total	True	False
[< 0.62]	0	0	0	0	0	0	0	0	0	0	0	0	0	0	0
[0.62–6.98]	0	5	0	0	0	0	0	0	0	0	0	0	5	5	0
[6.98–13.34]	0	0	0	0	0	0	0	0	0	0	0	0	0	0	0
[13.34–19.70]	0	1	0	3	0	0	0	0	0	0	0	0	4	3	1
[19.70–26.06]	0	0	0	1	8	0	0	0	0	0	0	0	9	8	1
[26.06–32.42]	0	0	0	0	0	8	0	0	0	0	0	0	8	8	0
[32.42–38.78]	0	0	0	0	0	0	5	1	0	0	0	0	6	5	1
[38.78–45.14]	0	0	0	0	0	0	0	2	0	0	0	0	2	2	0
[45.14–51.50]	0	0	0	0	0	0	0	1	0	0	0	0	1	0	1
[51.50–57.86]	0	0	0	0	0	0	0	0	0	1	0	0	1	1	0
[57.86–64.22]	0	0	0	0	0	0	0	0	0	0	1	0	1	1	0
[> 64.12]	0	0	0	0	0	0	0	0	0	0	0	0	0	0	0
Note	0	6	0	4	8	8	5	4	0	1	1	0	37	33	4
		MCD											Results		
Note	0	1	4	2	11	9	5	3	1	1	0	0	37	27	10
		QR											Results		
Note	2	3	1	3	10	7	5	4	1	1	0	0	37	29	8

Table 3. Improvement of *ARDCW* in *UQ* compared to *MCD* and *QR*

Model	Classification accuracy (%)		Misclassification error (%)		Progress (%)	Improvement compared to other models (%)			
	Test	Validate	Test	Validate		*MCD*	*ARDCW*	*QR*	Rank
MCD	0.69	0.73	0.31	0.27	0.04	–	– 22	– 6.8	3
ARDCW	0.77	0.89	0.23	0.11	0.12	22	–	14	1
QR	0.73	0.78	0.27	0.22	0.05	6.8	– 14	–	2

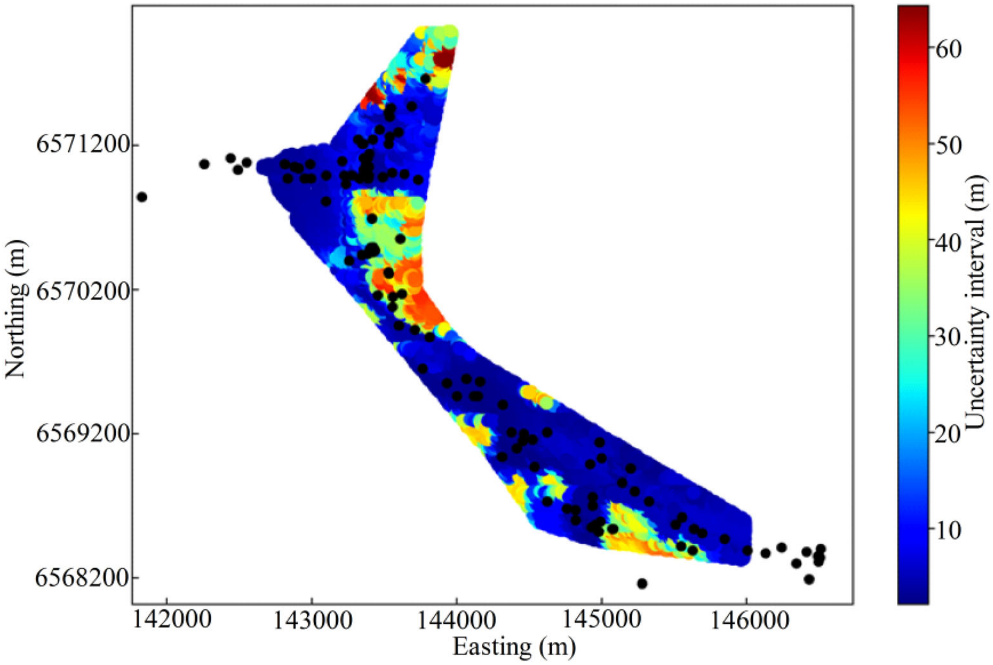

Figure 13. Estimated uncertainty intervals using *GWT* data (black dots) in the entirety of the study area.

many previously presented *GWT* models, which are intended for efficient decision support. Using the created 3D predictive model, the geospatial distribution of *GWT* and corresponding variations within subsurface geo-formations can be pursued. This concern can significantly influence the design of underground transport infrastructures for the city of Stockholm, where, in geo-engineering perspective the drainage of the *GWT* through tunnelling can cause ground settlements in the surrounding buildings. This phenomenon can be particularly problematic in weak soil/rock formations and manifest as a defective injection process. Moreover, the created model can decrease the risk of water inrush from excavation. By adding more geological data, the ability to recognize swelling clayey material which is a major threat in tunnelling projects can also be achieved. This implies that the presented *GWT* model is an indispensable tool for decision makers in urban development projects (e.g., building detached homes, roads, railways and bridges), where substantial land surface processes can be imposed.

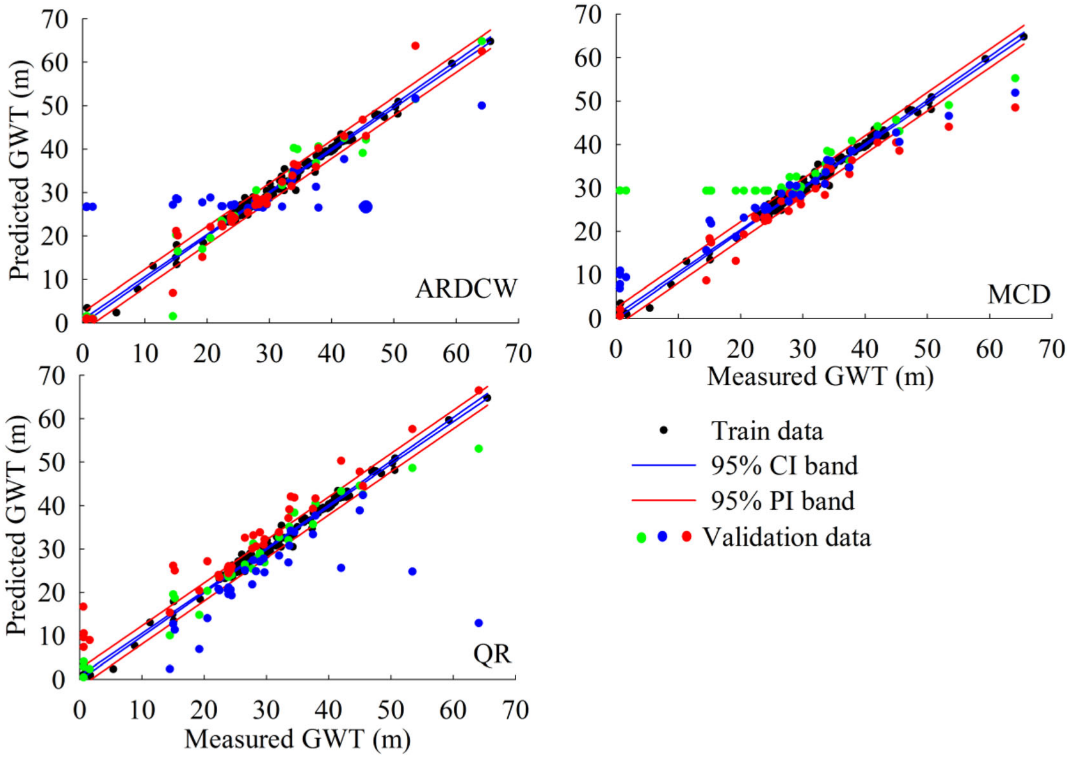

Figure 14. Comparative plots of the methods applied in *UQ* at 95% level for both *CI* and *PI*.

ACKNOWLEDGMENTS

The authors would like to express their special gratitude to Swedish Transport Administration through Better Interactions in Geotechnics (BIG), the Rock Engineering Research Foundation (BeFo) and Tyréns AB for supporting this research. We also wish to thank our colleagues, who provided insight and expertise that greatly assisted us in our research.

FUNDING

This work was supported by Rock Engineering Research Foundation (BeFo) (Grant Number BeFO 415), and Swedish Transport Administration through Better Interactions in Geotechnics (BIG) (Grant Number BIG A2019:17).

AVAILABILITY OF DATA AND MATERIALS

Data were made available after approval by the Swedish Transport Administration, and will not be shared to third party.

DECLARATIONS

CONFLICT OF INTEREST The authors have no known conflicts of interest to declare associated with this publication.

OPEN ACCESS

REFERENCES

Abbaszadeh, S. A., Kheiri, A., & Hamzeh, A. (2021a). Subsurface topographic modelling using geospatial and data driven algorithm. *ISPRS International Journal of Geo-Information, 10*(5), 341.

Abbaszadeh, S. A., Larsson, S., & Renkel, C. (2020). Artificial intelligence models to generate visualized bedrock level: A case study in Sweden. *Modeling Earth Systems and Environment, 6*, 1509–1528. https://doi.org/10.1007/s40808-020-00767-0.

Abbaszadeh, S. A., Shan, C., Zäll, E., & Larsson, S. (2021b). Spatial distribution modelling of subsurface bedrock using a developed automated intelligence deep learning procedure: A case study in Sweden. *Journal of Rock Mechanics and Geotechnical Engineering, 13*(6), 1300–1310.

Angiulli, F., & Fassetti, F. (2020). Uncertain distance–based outlier detection with arbitrarily shaped data objects. *Journal of Intelligent Information Systems, 57*, 1–24.

Asheghi, R., Hosseini, S. A., Saneie, M., & Abbaszadeh, S. A. (2020). Updating the neural network sediment load models using different sensitivity analysis methods: A regional application. *Journal of Hydroinformatics, 22*(3), 562–577.

Asheghi, R., Abbaszadeh, S. A., & Khorsand, Z. M. (2019). Prediction of uniaxial compressive strength of different quarried rocks using metaheuristic algorithm. *Arabian Journal for Science and Engineering, 44*, 8645–8659.

Atanassov, E., & Dimov, I. T. (2008). What Monte Carlo models can do and cannot do efficiently? *Applied Mathematical Modelling, 32*(8), 1477–1500.

Bárdossy, G., & Fodor, J. (2001). Traditional and new ways to handle uncertainty in geology. *Natural Resources Research, 10*, 179–187.

Barford, N. C. (1985). *Experimental measurements: Precision, error, and truth.* Wiley–Blackwell.

Barrio, R., Rodriguez, M., Abad, A., & Blesa, F. (2011). Breaking limits: The Taylor series method. *Applied Mathematics and Computation., 217*(20), 7940–7954.

Beven, K., & Binley, A. (1992). The future of distributed models: Model calibration and uncertainty prediction. *Hydrological Processes, 6*, 279–298.

Bizhanimanzar, M., Leconte, R., & Nuth, M. (2019). Modeling of shallow water table dynamics using conceptual and physically based integrated surface–water–groundwater hydrologic models. *Hydrology Earth System Science, 23*(5), 2245–2260.

Borgonovo, E. (2006). Measuring uncertainty importance: Investigation and comparison of alternative approaches. *Risk Analysis, 26*(5), 1349–1361.

Cacuci, D. G., & Ionescu-Bujor, M. (2004). A comparative review of sensitivity and uncertainty analysis of large–scale systems–II: Statistical methods. *Nuclear Science and Engineering, 147*(3), 204–217.

Chahbaz, R., Sadek, S., & Najjar, S. (2019). Uncertainty quantification of the bond stress–displacement relationship of shoring anchors in different geologic units. *Georisk: Assessment and Management of Risk for Engineered Systems and Geohazards, 13*(4), 276–283.

Chen, C., He, W., Zhou, H., Xue, Y., & Zhu, M. (2020). A comparative study among machine learning and numerical models for simulating groundwater dynamics in the Heihe River Basin, northwestern China. *Scientific Reports, 10*, 3904.

Chen, T., Fox, E., & Guestrin, C. (2014). Stochastic gradient hamiltonian monte carlo. In *Proceedings of international conference on machine learning* (pp. 1683–1691).

Cox, D. C., & Baybutt, P. (1981). Methods for uncertainty analysis: A comparative survey. *Risk Analysis, 1*(4), 251–258.

Cruzes, D. S., & Dyba, T. (2011). Research synthesis in software engineering: A tertiary study. *Information and Software Technology, 53*, 440–455.

Dietterich, T. G. (2000). Ensemble methods in machine learning. In *Multiple classifier systems, MCS 2000, Lecture notes in computer science,* 1857, 1–15.

Eisenhart, C., Ku, H. H., & Cole, R. (1983). Expression of the uncertainties of final measurement results: Reprints. *U.S. Department of Commerce/National Bureau of Standards,* NBS Special Pub. 644, Washington DC, USA.

Elam, K. R., & Rearden, B. T. (2017). Use of sensitivity and uncertainty analysis to select benchmark experiments for the validation of computer codes and data. *Nuclear Science and Engineering., 145*(2), 196–212.

Farrance, I., & Frenkel, R. (2012). Uncertainty of measurement: A review of the rules for calculating uncertainty components through functional relationships. *Clinical Biochemist Reviews, 33*(2), 49–75.

Foong, A. K., Burt, D. R., Li, Y., & Turner, R. E. (2019). Pathologies of factorized Gaussian and MC dropout posteriors in Bayesian neural networks. In *Proceedings of 4th workshop on Bayesian Deep Learning (NeurIPS 2019)*, abs/1909.00719, Vancouver, Canada.

Freitas, C. (2002). The issue of numerical uncertainty. *Applied Mathematical Modeling., 26*(2), 237–248.

Gal, Y., & Ghahramani, Z. (2016). Dropout as a Bayesian approximation: Representing model uncertainty in deep learning. In M. F. Balcan & K. Q. Weinberger (Eds.), *Proceedings of 33nd international conference on machine learning, ICML, NY, USA* (Vol. 48, pp. 1050–1059).

Geffray, C., Gerschenfeld, A., Kudinov, P., Mickus, I., Jeltsov, M., Kööp, K., Grishchenko, D., & Pointer, D. (2019). Verification and validation and uncertainty quantification. *Thermal Hydraulics Aspects of Liquid Metal Cooled Nuclear Reactors*, 383–405.

Ghaderi, A., Abbaszadeh Shahri, A. & Larsson, S. (2019) An artificial neural network based model to predict spatial soil type distribution using piezocone penetration test data (CPTu). *Bulletin of Engineering Geology and the Environment, 78*, 4579–4588. https://doi.org/10.1007/s10064-018-1400-9.

Glimm, J., & Sharp, D. H. (1999). Prediction and the quantification of uncertainty. *Physica D: Nonlinear Phenomena, 133*(1–4), 152–170.

Goodman, L. (1960). On the exact variance of products. *Journal of the American Statistical Association, 55*(292), 708–713.

Guillaume, J. H. A., Hunt, R. J., Comunian, A., Blakers, R. S., & Fu, B. (2016). Methods for exploring uncertainty in groundwater management predictions. In A. J. Jakeman, O. Barreteau, R. J. Hunt, J. D. Rinaudo & A. Ross (Eds.), *Integrated groundwater management* (pp. 711–737). Springer. https://doi.org/10.1007/978-3-319-23576-9_28.

Gärdenfors, P., & Sahlin, N. E. (1982). Unreliable probabilities, risk taking, and decision making. *Synthese, 53*(3), 361–386.

Huang, W., Zhao, D., Sun, F., Liu, H., & Chang, E. (2015). Scalable Gaussian process regression using deep neural networks. In *Proceedings of 24th international conference on artificial intelligence, IJCAI'15* (pp. 3576–3582).

Hauser, J., Wellmann, F., & Trefry, M. (2017). Water table uncertainties due to uncertainties in structure and properties of an unconfined aquifer. *Groundwater, 56*(2), 251–265. https://doi.org/10.1111/gwat.12577.

Hernandez–Lobato, J.M., & Adams, R. (2015). Probabilistic backpropagation for scalable learning of bayesian neural networks. In *Proceedings of 32nd international conference on machine learning, ICML* (Vol. 37, pp. 1861–1869).

Hernandez, S., & Lopez, J. L. (2020). Uncertainty quantification for plant disease detection using Bayesian deep learning. *Applied Soft Computing, 96*, 106597.

Hinton, E., Srivastava, N., Krizhevsky, A., Sutskever, I., & Salakhutdinov, R. (2012). Improving neural networks by preventing co–adaptation of feature detectors. arXiv:1207.0580.

Hirschefeld, L., Swanson, K., Yang, K., Barzilay, R., & Coley, C. W. (2020). Uncertainty quantification using neural networks for molecular property prediction. *Journal of Chemical Information and Modeling., 60*, 3770–3780.

Hu, L., & Jiao, J. J. (2010). Modeling the influences of land reclamation on groundwater systems: A case study in Shekou peninsula, Shenzhen, China. *Engineering Geology, 114*(3–4), 144–153.

Huber, M. (2016). Reducing forecast uncertainty by using observations in geotechnical engineering. *Probabilistic Engineering Mechanics, 45*, 212–219.

Jiang, C., Zheng, J., & Han, X. (2018). Probability–interval hybrid uncertainty analysis for structures with both aleatory and epistemic uncertainties: A review. *Structural and Multidisciplinary Optimization, 57*, 2485–2502.

Jin, X., Xu, C. Y., Zhang, Q., & Singh, V. P. (2010). Parameter and modeling uncertainty simulated by GLUE and a formal Bayesian method for a conceptual hydrological model. *Journal of Hydrology, 383*, 147–155.

Kabir, H. D., Khosravi, A., Hosen, M. A., & Nahavandi, S. (2018). Neural network–based uncertainty quantification: A survey of methodologies and applications. *IEEE Access., 6*, 36218–36234.

Kadanoff, L. P. (2009). More is the same, phase transitions and mean field theories. *Journal of Statistical Physics, 137*(5–6), 777–797.

Kennedy, M. C., & O'Hagan, A. (2001). Bayesian calibration of computer models. *Journal of the Royal Statistical Society, Series B (Statistical Methodology), 63*(3), 425–464.

Keogh, E., & Kasetty, S. (2003). On the need for time series data mining benchmarks: A survey and empirical demonstration. *Data Mining and Knowledge Discovery, 7*, 349–371.

Klotz, D., Kratzert, F., Gauch, M., Sampson, A. K., Brandstetter, J., Klambauer, G., Hochreiter, S., & Nearing, G. (2021). Uncertainty estimation with deep learning for rainfall–runoff modeling. Hydrology and Earth System Science Discussion. https://doi.org/10.5194/hess-2021-154.

Krzywinski, M., & Altman, N. (2013). Points of significance: Importance of being uncertain. *Nature Methods, 10*(9), 809–810.

Lakshminarayanan, B., Pritzel, A., & Blundell, C. (2017). Simple and scalable predictive uncertainty estimation using deep ensembles. In *Proceedings of 31st international conference on neural information processing systems, NIPS'17* (pp. 6405–6416).

Leavesley, G. H., Lichty, R. W., Troutman, B. M., & Saindon, L. G. (1983). Precipitation-runoff modeling system user's manual. *Water-resources investigations report* 83–4238, USGS, Water division, USA. https://doi.org/10.3133/wri834238.

Legates, D. R., & McCabe, G. J. (1999). Evaluating the use of ''goodness–of–fit'' measures in hydrologic and hydroclimatic model validation. *Water Resource Research, 35*(1), 233–241.

Li, F., Zhu, J., Deng, X., Zhao, Y., & Li, S. (2018). Assessment and uncertainty analysis of groundwater risk. *Environmental Research, 160*, 140–151.

Loquerico, A., Segu, M., & Scaramuzza, D. (2020). A general framework for uncertainty estimation in deep learning. *IEEE Robotics and Automation Letters, 5*(2), 3153–3160.

MacKay, D. J. C. (1992). A practical Bayesian framework for backpropagation networks. *Neural Computation, 4*(3), 448–472.

Middlemis, H., & Peeters, L. J. M. (2018). Uncertainty analysis—Guidance for groundwater modelling within a risk management framework. *Report of information guidelines explonatory note*, IESC on Coal Seam Gas and Large Coal Mining Development, Department of the Environment and Energy, Commonwealth of Australia, 77P. https://doi.org/10.13140/RG.2.2.34589.36323.

Mohammadi, K. (2009). Groundwater table estimation using MODFLOW and artificial neural networks. In R.J. Abrahart, L.M. See, & D.P. Solomatine (Eds.), *Practical hydroinformatics* (Vol. 68, pp. 1287–138), Springer. https://doi.org/10.1007/978-3-540-79881-1_10.

Morgan, M. G., & Henrion, M. (1990). *Uncertainty: A guide to dealing with uncertainty in quantitative risk and policy analysis*. Cambridge University Press.

Nash, J. E., & Sutcliffe, J. V. (1970). River flow forecasting through conceptual models part I—A discussion of principles. *Journal of Hydrology, 10*, 282–290.

Neal, R. M. (2012). Bayesian learning for neural networks. *Lecture notes in statistics*, 118, Springer. https://doi.org/10.1007/978-1-4612-0745-0.

Parry, S., Baynes, F. J., Culshaw, M. G., Eggers, M., Keaton, J. R., Lentfer, K., Novotny, J., & Paul, D. (2014). Engineering geological models: An introduction: IAEG commission 25. *Bulletin of Engineering Geology and the Environment, 73*, 689–706.

Quinonero-Candela, J., Rasmussen, C. E., Sinz, F., Bousquet, O., & Schölkopf, B. (2006). Evaluating predictive uncertainty challenge. *Lecture Notes in Computer Science, 3944*, 1–27.

Rushton, K. R. (2003). *Groundwater hydrology: Conceptual and computational models*. Wiley.

Sahoo, S., & Russo, T. A. (2017). Machine learning algorithms for modeling groundwater level changes in agricultural regions of the U.S. *Water Resource Research, 53*(5), 3878–3895.

Salvo, C. D., Mancini, M., Cavinato, G. P., Moscatelli, M., Simionato, M., Stigliano, F., Rea, R., & Rodi, A. (2020). A 3D geological model as a base for the development of a conceptual groundwater scheme in the area of the Colosseum (Rome, Italy). *Geosciences, 10*, 266.

Sepulveda, N., & Doherty, J. (2015). Uncertainty analysis of a groundwater flow model in east-central Florida. *Groundwater, 53*(3), 464–474.

Shumway, R. H. (1988). *Applied statistical time series analysis*. Englewood Cliffs.

Srivastava, N., Hinton, G., Krizhevsky, A., Sutskever, I., & Salakhutdinov, R. (2014). Dropout: A simple way to prevent neural networks from overfitting. *Journal of Machine Learning Research, 15*(56), 1929–1958.

Stedinger, J. R., Vogel, R. M., Lee, S. U., & Batchelder, R. (2008). Appraisal of the generalized likelihood uncertainty estimation (GLUE) method. *Water Resource Research, 44*(12), W00B06.

Tacher, L., Pomian-Srzednicki, I., & Parriaux, A. (2006). Geological uncertainties associated with 3D subsurface models. *Computers & Geosciences, 32*, 212–221.

Tang, Y., Zhou, J., Yang, P., Yan, J., & Zhou, N. (2017). *Groundwater engineering*. Springer. https://doi.org/10.1007/978-981-10-0669-2.

Taper, M. L., & Ponciano, J. M. (2016). Evidential statistics as a statistical modern synthesis to support 21st century science. *Population Ecology, 58*, 9–29.

Uusitalo, L., Lehikoinen, A., Helle, I., & Myberg, K. (2015). An overview of methods to evaluate uncertainty of deterministic models in decision support. *Environmental Modelling Software, 63*, 24–31.

Vrugt, J. A., & Robinson, B. A. (2007). Treatment of uncertainty using ensemble methods: Comparison of sequential data assimilation and Bayesian model averaging. *Water Resource Research, 43*(1), W01411.

Waldmann, E. (2018). Quantile regression: A short story on how and why. *Statistical Modelling, 18*(3–4), 203–218.

Wan, L., Zeilar, M., Zhang, S., LeCun, Y., & Fergus, R. (2013). Regularization of neural networks using DropConnect. In *Proceedings of ICML'13, international conference on machine learning (PMLR)* (Vol. 28, No. 3, pp. 1058–1066).

Weerts, A. H., Winsemius, H. C., & Verkade, J. S. (2011). Estimation of predictive hydrological uncertainty using quantile regression: Examples from the National Flood Forecasting System (England and Wales). *Hydrology and Earth System Sciences, 15*(1), 255–265.

Whitman, R. V. (2000). Organizing and evaluating the uncertainty in geotechnical engineering. *Journal of Geotechnical & Geoenvironmental Engineering, 126*(7), 583–593.

Wilcox, B. P., Rawls, W. J., Brakensiek, D. L., & Wight, J. R. (1990). Predicting runoff from rangeland catchments: A comparison of two models. *Water Resources Research, 26*(10), 2401–2410.

Willmott, C.J. (1984). On the evaluation of model performance in physical geography. In G.L. Gaile & C.J. Willmott (Eds.), *Spatial statistics and models. Theory and decision* (Vol. 40, pp: 443–460). Springer. https://doi.org/10.1007/978-94-017-3048-8_23.

Wu, J., & Zeng, X. (2013). Review of the uncertainty analysis of groundwater numerical simulation. *Chinese Science Bulletin, 58*, 3044–3052.

Wunsch, A., Liesch, T., & Broda, S. (2020). Groundwater level forecasting with artificial neural networks: A comparison of LSTM, CNN and NARX. *Hydrology and Earth System Science Discussion*. https://doi.org/10.5194/hess-2020-552.

WWAP (World Water Assessment Programme). (2012). Managing water under uncertainty and risk. *The United Nations World Water Development Report*, 1, 417, UNESCO, Paris.

Xu, Y., & Goodacre, R. (2018). On splitting training and validation set: A comparative study of cross-validation, bootstrap and systematic sampling for estimating the generalization performance of supervised learning. *Journal of Analysis and Testing, 2*, 249–262. https://doi.org/10.1007/s41664-018-0068-2.

Yager, R. R. (1996). On the inclusion of variance in decision making under uncertainty. *International Journal of Uncertainty, Fuzziness and Knowledge-Based Systems, 04*(05), 401–419.

Yan, J., Liu, Y., Han, S., Wang, Y., & Feng, S. (2015). Reviews on uncertainty analysis of wind power forecasting. *Renewable and Sustainable Energy Reviews, 52*, 1322–1330.

Yan, S., Yu, S., Wu, Y., Pan, D., & Dong, J. (2018). Understanding groundwater table using s statistical model. *Water Science and Engineering, 11*(1), 1–7.

Yang, Y., Wang, H. X., & He, X. (2016). Posterior inference in Bayesian quantile regression with asymmetric Laplace likelihood. *International Statistical Review, 84*(3), 327–344.

Yeh, T., Mao, D., Zha, Y., Wen, J., Wan, L., Hsu, K., & Lee, C. (2015). Uniqueness, scale, and resolution issues in groundwater model parameter identification. *Water Science and Engineering, 8*(3), 175–194.

Yin, J., Medellin-Azuara, J., Escriva-Bou, A., & Liu, Z. (2021). Bayesian machine learning ensemble approach to quantify model uncertainty in predicting groundwater storage change. *Science of The Total Environment, 769*, 144715.

Zhang, J., Yin, J., & Wang, R. (2020). Basic framework and main methods of uncertainty quantification. *Materia Problems in Engineering, 2020*, 6068203.

Zhang, X., Xiao, H., Gomez, T., & Coutier-Delgosha, O. (2021). Evaluation of ensemble methods for quantifying uncertainties in steady–state CFD applications with small ensemble sizes. *Computer & Fluids, 203*, 104530.

Zhu, Y., Zabaras, N., Koutsourelakis, P. S., & Perdikaris, P. (2019). Physics-constrained deep learning for high-dimensional surrogate modeling and uncertainty quantification without labelled data. *Journal of Computational Physics, 394*, 56–81.